JCI insight

Hypercapnia alters stromal-derived Wnt production limiting β-catenin signaling and proliferation in alveolar type 2 cells

Laura A. Dada, Lynn C. Welch, Natalia D. Magnani, Ziyou Ren, Hyebin Han, Patricia L. Brazee, Diego Celli, Annette S. Flozak, Anthea Weng, Mariana Maciel Herrerias, Vitalii Kryvenko, István Vadász, Constance E. Runyan, Hiam Abdala-Valencia, Masahiko Shigemura, S. Marina Casalino-Matsuda, Alexander V. Misharin, G.R. Scott Budinger, Cara J. Gottardi, Jacob I. Sznajder

JCI Insight. 2023. https://doi.org/10.1172/jci.insight.159331.

Research In-Press Preview Cell biology Pulmonology

Graphical abstract

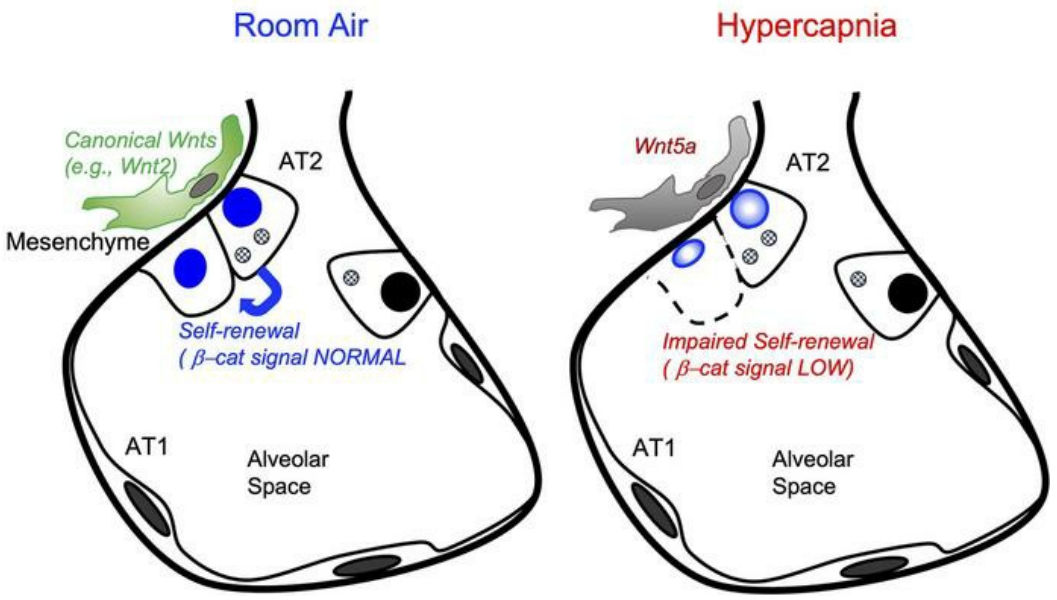

Hypercapnia alters stromal-derived Wnt production limiting β-catenin signaling and proliferation in alveolar type 2 cells

Laura A. Dada[1]*, Lynn C. Welch[1], Natalia D. Magnani[1], Ziyou Ren[1], Hyebin Han[1], Patricia L. Brazee[1], Diego Celli[1], Annette S. Flozak[1], Anthea Weng[1], Mariana Maciel-Herrerias[1], Vitalii Kryvenko[1,2], István Vadász[2], Constance E. Runyan[1], Hiam Abdala-Valencia[1], Masahiko Shigemura[1], S. Marina Casalino-Matsuda[1], Alexander V. Misharin[1], G.R. Scott Budinger[1], Cara J. Gottardi[1]*, Jacob I. Sznajder[1]

[1]Pulmonary and Critical Care Medicine, Northwestern Feinberg School of Medicine. Chicago, IL. 60611. USA

[2]Justus Liebig University, Universities of Giessen and Marburg Lung Center, Member of the German Center for Lung Research, Department of Internal Medicine, Giessen, Germany; The Cardio-Pulmonary Institute, Giessen, Germany

**Corresponding authors*

Laura A. Dada
303 E Superior St
Simpson-Querrey 5-405
Chicago, IL 60611, USA
Email: lauradada@northwestern.edu
Phone: 312-503-5397

Cara J. Gottardi
303 E Superior St
Simpson-Querrey 5-525
Chicago, IL 60611, USA
Email: c-gottardi@northwestern.edu
Phone: 312-503-4123

Conflict of Interest: The authors have declared that no conflict of interest exists

Short title: Hypercapnia inhibits AT2 proliferation

Abstract

Persistent symptoms and radiographic abnormalities suggestive of failed lung repair are among the most common symptoms in patients with COVID-19 after hospital discharge. In mechanically ventilated patients with ARDS secondary to SARS-CoV-2 pneumonia, low tidal volumes to reduce ventilator-induced lung injury necessarily elevate blood CO_2 levels, often leading to hypercapnia. The role of hypercapnia on lung repair after injury is not completely understood. Here, using a mouse model of hypercapnia exposure, cell lineage-tracing, spatial transcriptomics and 3D-cultures, we show that hypercapnia limits β-catenin signaling in AT2 cells, leading to their reduced proliferative capacity. Hypercapnia alters expression of major Wnts in PDGFRα$^+$-fibroblasts from those maintaining AT2 progenitor activity towards those that antagonize β-catenin signaling thereby limiting progenitor function. Constitutive activation of β-catenin signaling in AT2 cells or treatment of organoid cultures with recombinant WNT3A protein bypasses the inhibitory effects of hypercapnia. Inhibition of AT2 proliferation in hypercapnic patients may contribute to impaired lung repair after injury, preventing sealing of the epithelial barrier, increasing lung flooding, ventilator dependency and mortality.

Introduction

As of this writing, more than 651 million people have been diagnosed globally with Coronavirus Disease 2019 (COVID-19) and nearly 6.7 million people have died (https://coronavirus.jhu.edu). Severe COVID-19 presents as acute respiratory distress syndrome (ARDS) where injury of the alveolar epithelial barrier causes flooding of the alveolar space and pulmonary edema, which in severe cases may require mechanical ventilation (1, 2). In the US alone, there are currently more than 90 million survivors of COVID-19. Studies focused on post-acute sequelae of COVID-19 (PASC) suggest persistent respiratory symptoms, where radiographic abnormalities and need for supplemental oxygen are common in survivors of COVID-19, particularly those requiring high flow oxygen therapy or mechanical ventilation (3). These persistent symptoms suggest that failure of normal lung repair mechanisms can prevent complete recovery of lung function in a substantial fraction of COVID-19 survivors with significant public health impact.

Low tidal volume ventilation is a proven strategy to reduce the incidence and severity of ventilator-induced lung injury (4-6). The alveolar hypoventilation associated with low tidal volumes necessarily increases blood CO_2 levels, described clinically as hypercapnia. Hypercapnia is exacerbated by increased steady state carbon dioxide production and dead space ventilation common in patients with severe SARS-CoV-2 pneumonia and ARDS (4, 6, 7). We and others found that exposure to hypercapnia activates signaling pathways detrimental to alveolar epithelial wound healing and migration (4-10), but mechanisms by which hypercapnia impairs epithelial repair remain incompletely understood.

While baseline turnover in the alveolar epithelium is slow, alveolar injury results in rapid and robust alveolar type 2 (AT2) cell proliferation and differentiation to restore barrier function and gas exchange (11-13). During homeostasis and after lung injury, lineage tracing studies suggest that AT2 cells self-renew and serve as progenitor cells for alveolar type 1 (AT1) cells (13-16). Our group was among the first to report that Wnt/β-catenin (βcat) signaling regulates both the survival and migration of AT2 cells post-injury (17). Recent studies suggest that a subset of AT2 cells with activated Wnt/βcat-signaling display higher progenitor activity than the Wnt-inactive bulk population of AT2 cells (11, 16, 18, 19). Such differences in AT2 progenitor subsets are

thought to be spatially induced in response to signals from the niche. For example, single cell RNA-sequencing data revealed that PDGFRα fibroblasts express Wnts, suggesting they might control the local activation of βcat AT2 cells (19-21), but the precise molecular signals and stromal cells that select AT2 progenitors are still undefined (16, 19, 21). Furthermore, whether and how signals responsible for maintenance and repair of the AT2/mesenchymal niche are affected by hypercapnia in the injured lung are not known.

Here, we determined the effects of hypercapnia on AT2 progenitor capacity using unbiased RNA-sequencing analysis of flow-sorted AT2 cells and validation with lineage-labelled AT2 cells subjected to *ex vivo* organoid growth. Our findings suggest that hypercapnia limits AT2 cell β-catenin signaling and progenitor function by altering Wnt-expression in surrounding niche cells. We show that hypercapnia skews expression of PDGFRα$^+$/stroma-derived Wnt signals away from those typically known to activate βcat signaling (e.g., canonical *Wnt2*), and towards those historically shown to drive morphogenetic processes independently of βcat (e.g., non-canonical *Wnt5a*). We validate this model showing WNT5A inhibits βcat signaling in primary AT2 *ex vivo* cultures. We also show that *Pdgfra/Wnt2* cells are spatially closer to AT2 cells than *Pdgfra/Wnt5a* cells under baseline conditions, where flow-sorted PDGFRα$^+$ cells can be sub-divided into populations expressing Wnts non-uniformely (e.g., *Wnt2*$^+$*, Wnt5a*$^+$*, Wnt2*$^+$*/Wnt5*$^+$*, Wnt2*$^-$*/Wnt5a*$^-$*),* suggesting their spatial arrangement could direct distinct AT2 cell behaviors in the distal lung. Importantly, hypercapnia blurs this spatial separation by upregulating *Wnt5a*$^+$ in *Pdgfra/Wnt2*$^+$ cells, causing the *Wnt5a*$^+$ signal to be closer to AT2 cells. Altogether, these data suggest a mechanism by which hypercapnia may slow lung repair after injury, with broad implications for understanding how stromal-derived Wnt signals direct alveolar epithelial behaviors during repair.

Results

Hypercapnia limits AT2 proliferation in vitro and in vivo

To assess the effect of hypercapnia on AT2 cell progenitor capacity, we employed a 3D-organoid model. Mouse primary AT2 cells were isolated by fluorescence-activated cell sorting (FACS) ($EPCAM^+MHCII^+$) from leukocyte/endothelial cell-depleted lung homogenates of wild-type mice as described (22, 23) (**Supplemental Figure 1A),** or from $Sftp^{CreERT2}:R26R^{EYFP}$ mice as $EPCAM^+YFP^+$ (**Supplemental Figure 1B**). In $Sftp^{CreERT2}:R26R^{EYFP}$ mice*,* tamoxifen administration permanently induces the expression of YFP specifically in AT2 cells and their progeny (18). To establish lung organoids, AT2 cells were embedded in Matrigel in the presence of mesenchymal cells in a 1:10 ratio **(Figure 1A**). In normocapnic conditions (5% CO_2 pH:7.4, NC), sphere-like colony formation was seen typically between 5-7 days, which continued for up to 21 days (**Figure 1, A and B**). When cultures were started in the presence of high CO_2 (20% CO_2 pH:7.4, HC), we did not observe organoid formation (data not shown), suggesting hypercapnia profoundly affects AT2 cell colony formation. To better assess the consequences of hypercapnia on AT2 progenitor activity, we grew organoids for 7 days in control media before switching cultures to conditioned media equilibrated to either 5 or 20% CO_2 for an additional 7-14 days (**Figure 1, A-E**). Under these conditions, small spheres can be observed at 7 days (median diameter approx. 72 μm) in which AT2 cells have not yet started to differentiate while larger spheres are present at 14 and 21 days (**Figure 1B**). Hypercapnia significantly decreased average organoid diameter compared to organoids grown in normocapnia and reduced AT2 clonogenicity (Colony Forming Efficiency (CFE)) (**Figure 1, C and D and Supplemental figure 2A)**. Whole organoids were fixed and visualized using Surfactant protein C (SFTPC) and Podoplanin to indicate AT2 and AT1 cells, respectively. After 14 and 21 days in culture in normocapnic conditions, organoids displayed a characteristic structure with central AT1 cells surrounded by peripheral AT2 cells; during hypercapnia, few AT2 cells were observed with almost no AT1 cell marker detection (**Figure 1E**). To determine whether the effects of hypercapnia on AT2 proliferation were reversible, we switched organoids grown under hypercapnia into normocapnia as described in **Supplemental Figure 2B**. Results show that 7 days of normocapia can partially reverse the effects of hypercapnia on organoid growth **(Supplemental Figure 2, C-D)**.

To assess the effects of hypercapnia on proliferation *in vivo*, mice were exposed for 21 days to either breathing room-air (RA) or 10% CO_2 (HC). Hypercapnia limited the proliferative capacity of AT2 cells in mice, as evidenced by fewer $SFTPC^+$-AT2 cells co-expressing the proliferation marker, Ki67 (**Figure 2, A and B**).

Hypercapnia inhibits Wnt/βcat signaling in AT2 cells

To determine how hypercapnia limits AT2 progenitor capacity and differentiation, we interrogated transcriptional differences in bulk-sorted AT2 cells isolated from mice exposed either to room air or hypercapnia. Mice were exposed to high CO_2 for 7 and 21 days and AT2 cells were isolated from single cell suspensions as described above, RNA was isolated and bulk RNASeq was performed as previously described (24, 25). After 7 days of hypercapnia, only 15 differentially expressed genes (DEG) were identified compared to AT2 cells isolated from mice kept at room air (**Figure 2, C and D**). After 21 days of exposure to hypercapnia, over 1200 DEG were identified compared to room-air mice (**Figure 2E**), where enrichment analysis of biological processes revealed hypercapnia inhibits lipid synthesis/metabolism, lysosomal pathways, and canonical Wnt signaling (**Figure 2F**). Specifically, hypercapnia limited the expression of genes coding for essential regulators of AT2 lineage (*Etv5, Abca3*) (26, 27), functional markers of AT2 cell function (*Sftpc, Nkx2.1*) (26, 28) and lipid metabolism (*Fabp5, Hmgcr*) (26, 28) (**Supplemental Figure 3, A-F),** suggesting an impairment of AT2 cell maturation and function**.** Decreased expression of *Spftc/*SFTPC were confirmed at both RNA and protein levels, and by counting the number SFTPC positive cells in lung tissue slides from mice exposed for 21d to hypercapnia or room-air (**Supplemental Figure 3, G-J**). Fibroblast growth factor receptor 2 (*Fgfr2)*, which is necessary for AT2 cell maintenance and self-renewal (29, 30), was decreased by 50% in AT2 cells after 21 days of hypercapnia compared to room-air exposed mice (**Supplemental Figure 3K**), consistent with our evidence that hypercapnia attenuates AT2 proliferative capacity.

Since Wnt signaling plays a major role in lung homeostasis and repair after injury (18, 19, 31), we interrogated established target genes and components related to this pathway. We found hypercapnia inhibited expression of *Ctnnb1* itself, as well as *Nkd1* (a known target) (32) and *Wls* (required for Wnts secretion) (33), and increased expression of *Wif1* (34), a negative feed-back regulator of Wnt/βcat signaling (**Figure 2, G-J**). We confirmed this finding in AT2 cells isolated from mice exposed to hypercapnia for 21 days by monitoring *Axin2* expression,

a universal target of Wnt/βcat signaling whose expression reports pathway activation across a range of cell types and tissues (18, 19, 35) (**Figure 3A**). Hypercapnia also limited the number of *Axin2*-expressing AT2 cells (*Sftpc*$^{+}$*Axin2*$^{+}$) using multiplexed in situ hybridization of wild-type mouse lung sections (**Figure 3, B and C and Supplemental Figure 4A**) with independent confirmation by using the βcat signaling reporter mouse *Axin2*$^{CreERT2\text{-}TdTom}$ (**Figure 3D and Supplemental Figure 4E**). In this Wnt/βcat-responsive fluorescent reporter line, *Axin2*$^{TdTomato+}$ cells are restricted to the distal epithelium and surrounding mesenchyme at E13.5, where this pattern continues through adulthood (18). As with previous reports, we isolated bright populations of *Axin2*$^{TdTomato\text{-}HIGH}$ expressing cells that are SFTPC-negative, as well as dim *Axin2*$^{TdTomato\text{-}DIM}$ SFTPC^{+} AT2 cells (**Supplemental Figure 4, B-D**). Together, these data suggest hypercapnia antagonizes AT2 progenitor activity by limiting βcat signaling within AT2 cells.

Hypercapnia skews stromal-derived Wnts towards a βcat signaling inhibitory environment

To determine the mechanism by which hypercapnia limits βcat signaling activity in AT2 cells, we first interrogated our AT2 bulk RNAseq data set for altered expression of Wnt genes, given previous evidence that hyperoxic lung injury upregulates a set of AT2 cell Wnts that could alter "bulk" AT2 behavior (19) and that short-term hypercapnia up-regulates Wnt7a in mouse lung homogenates (36). However, *Wnt7b,* one of the most highly expressed AT2 cell Wnts (19), was not altered by hypercapnia (data not shown). While *Wnt3a* and *Wnt4* expression were mildly reduced by hypercapnia, they were minimally expressed and thus were not validated by RNA-FISH (not shown) or single cell data (25). Since stromal niche cells proximal to AT2 cells are critical for AT2 proliferation and differentiation to AT1 cells (13, 16), we sought to assess whether hypercapnia limits alveolar epithelial cell renewal by modifying Wnts produced from adjacent fibroblasts. We isolated PDGFRα-expressing fibroblasts (CD45^{-}CD31^{-}EPCAM^{-}PDGFRα^{+}) from mice exposed to high CO_2 for 10 days and analyzed their transcriptomic profiles, identifying ~310 genes differentially expressed by exposure to hypercapnia **(Supplemental Figure 5)**. This analysis revealed robust expression of a number of Wnts previously identified in our scRNA-seq data sets as fibroblast-enriched (*Wnt2, -2b, -9a, -4, -5a* and *-11*) (25), where *Wnt5a* and *Wnt2* were the most abundant **(Figure 4A)**. Hypercapnia increased *Wnt5a* (significantly), a Wnt typically known to antagonize βcat signaling and promote cell shape and polarized behaviors (37, 38). Conversely, expression of *Wnt2*, which has been described to activate Wnt/βcat signaling in rat lung fibroblasts

in NIH-3T3 (39, 40) trended downwards. The hypercapnia-induced *Wnt5a*-increase and *Wnt2*-decrease were independently confirmed by isolating mRNA from PDGFRα^{+} fibroblasts (**Figure 4, B and C).** To interrogate signals downstream of hypercapnia that can enhance *Wnt5a* expression, we preincubated MLg 2908 mouse lung fibroblasts with pathway inhibitors before exposure to 5% or 20% CO_2. We found that hypercapnia-induced *Wnt5a* elevation was sensitive to MAPK inhibition as assessed by the use of PD98059 and UO126 (highly selective inhibitors of MEK1/2 and the MAPK cascade) (**Figure 4D)**. These data are consistent with our previous evidence that acute hypercapnic exposure leads to activation of MAPK-signaling (41), and suggest *Wnt5a* may be a target of MAPK signals.

Validating whether particular Wnts are βcat "activating" or "inhibiting" is important, given conflicting reports on the role of WNT5A in AT2 progenitor behavior (19, 37, 42). As is typically observed in established reporter assays, we found recombinant WNT3A (rWNT3A) promoted βcat signaling in alveolar epithelial (A549) cells, whereas WNT5A did not **(Figure 5A)**. rWNT3A was used as a canonical Wnt/βcat activator (positive control), since validated recombinant WNT2 (i.e., purified from mammalian cell culture secretions) is not available (R&D Systems; Bio-techne). We independently confirmed these findings by expressing Wnts via adenoviral transduction of primary AT2 cell cultures using an established affinity precipitation-based assay to capture and quantify the cadherin-free signaling fraction of βcat (**Figure 5, B and C**) (43). This experiment showed that irrespective of AT2 cell seeding density, WNT5A limits the cytosolic pool of βcat available for signaling (**Figure 5C**). Conversely, WNT3A elevates the cytosolic pool of βcat in AT2 cells, consistent with its longstanding role as an activator of βcat signaling. Together, these data show that WNT5A antagonizes βcat signaling in cultured AT2 cells and raise the possibility that hypercapnia may limit the progenitor capacity of AT2 cells through stromal-derived WNT5A.

Activation of βcat-signaling rescues AT2 progenitor activity during hypercapnia

While hypercapnia can limit βcat signaling activity, the aggregate effects of hypercapnia are likely to be pleotropic. Thus, we sought to test whether the ability of hypercapnia to limit AT2 progenitor capacity could be offset by forced-activation of β-catenin signaling. The most convenient Wnt/βcat signaling pathway activators work by inhibiting glycogen synthase kinase-3β (GSK-3β), the central inhibitory kinase in this pathway (44).

GSK-3β inhibitors antagonize βcat phosphorylation and degradation, allowing βcat to accumulate in the nucleus and trans-activate Wnt signals. As such, 24 h after switching the media to hypercapnia, organoids were incubated in the presence or absence of the GSK-3β inhibitor CHIR99021 (CHIR, 20nM). CHIR did not significantly increase organoid size in normocapnia but significantly rescued organoid growth during exposure to hypercapnia **(Supplemental Figure 6, A and B**). Since GSK3 has numerous cellular targets with roles in many signaling processes, we also assessed whether the anti-progenitor effects of hypercapnia could be rescued by constitutively activating βcat signaling in AT2 cells using *Sftpc*^{CreERT2}*:Ctnnb1*$^{Exon3fl/+}$*:R26R*^{EYFP} mice (45). In these mice, Cre-dependent removal of a phospho-degron in exon3 of the βcat gene (*Ctnnb1*) generates a constitutively active form of βcat. Remarkably, the increase in organoid size by constitutively active βcat was completely refractory to the anti-proliferative effects of hypercapnia (**Figure 6, A and B).** We further asked whether the anti-progenitor effects of hypercapnia could be bypassed by providing exogenous, extracellular Wnt proteins. We found WNT3A significantly enhanced organoid growth under both normocapnia and hypercapnia conditions, whereas WNT5A limited organoid growth as expected **(Figure. 6, C and D).** Altogether, these data show that the anti-progenitor effects of hypercapnia are reversible and can be offset by elevating βcat signaling within AT2 cells or by adding exogenous Wnts.

*Hypercapnia alters the spatial distribution of Wnt e*xpression in AT2-niche cells

Given recent evidence that the AT2 cell niche may comprise as few as 1-2 stromal cells to modulate βcat signaling in AT2 progenitor cells (19, 21) and to address how hypercapnia limits AT2 progenitor function, we sought to measure the spatial proximity of *Wnt2* and *Wnt5a* signal to *Sftpc*$^{+}$-AT2 cells RNA-FISH. We focused on *Wnt2* for comparison with *Wnt5a* as it is one of the most abundant stromal-derived Wnts (21, 25) and is known to activate βcat signaling across diverse cell types (46, 47). Given that WNT5A can antagonize the βcat signaling pool in AT2 cells (**Figure 5),** we reasoned βcat-activating and -inhibiting Wnts might be spatially separated in the AT2 niche to control AT2 progenitor versus differentiation decisions. By converting RNA-FISH signal to objects (i.e., "spots") based on signal intensity (see Methods), we measured median shortest distances between signal pairs **(Figure 7, A and B).** We found that while both *Wnt2*- and *Wnt5a*-expressing *Pdgfra*$^{+}$ stromal cells are spatially proximal to *Sftpc*$^{+}$-AT2 cells, in normocapnic cells the *Wnt2* signal is significantly closer than *Wnt5a* **(**40 vs. 30% < 6μm respectivelly**, Supplemental Figure 7)**. We next asked whether the

spatial proximity of these Wnts was altered by hypercapnia. Remarkably, we found that hypercapnia led to a greater percentage of *Wnt5a* signal within the first distance bins (6μm), while the *Wnt2* signal did not significantly change **(Figure 7, C and D).** As expected, hypercapnia did not change the proximity of *Pdgfra* signal to *Sftpc* (**Figure 7E**). Collectively, these data suggest that hypercapnia increases *Wnt5a* expression, particular within the AT2 cell-proximal zone normally occupied by *Wnt2*.

To further interrogate our model of spatially separated βcat-activating versus βcat-inhibitory Wnts, we asked whether *Pdgfra*$^{+}$ stromal cells are uniformly *Wnt2/Wnt5a*-double-positive or instead comprise Wnt heterogeneity. For this, we used an imaging method that would allow visualization of the entire *Pdgfra*$^{+}$ cell population, rather than being limited to a 15μm thickness of lung frozen section. We isolated PDGFRα^{+} cells by flow cytometry and performed RNA-FISH analysis after cytospin. Interestingly, we found the PDGFRα^{+} cells could be distinguished as 4-subtypes regarding *Wnt2/Wnt5a* expression: *Wnt2*$^{+}$, *Wnt5a*$^{+}$, *Wnt2/Wnt5a*$^{++}$ and *Wnt2/Wnt5a*-negative **(Supplemental Figure 7 A-C and Figure 8A)**. While PDGFRα^{+} cells no doubt express other Wnts, the results showed that this population is not uniformly positive for both *Wnt2* and *Wnt5a*. Together with the evidence that these Wnts show different average distances from AT2 cells in lung sections, these data suggest that PDGFRα^{+} stroma cells establish a spatial code of βcat-activating versus -inhibitory Wnt ligands to narrowly control the AT2 cell proliferative zone of the alveolus. We then sought to determine whether hypercapnia could alter the relative abundance of *Wnt2/Wnt5a/Pdgfra* subsets by performing RNA-FISH analysis on flow-sorted PDGFRα^{+} cells harvested from three-independent mice subjected to hypercapnia vs room air. We observed a significant increase in the *Wnt2/Wnt5a*$^{+}$ subpopulation, which may come at the expense of *Wnt2*$^{+}$ and *Wnt2*$^{-}$*Wnt5a*$^{-}$ subpopulations **(Figure 8, B and C).** Thus, AT2 cells reside within a niche PDGFRα^{+} stroma cells that are heterogenous regarding to *Wnt2* and *Wnt5a* expression. As *Pdgfra*$^{+}$*/Wnt2*$^{+}$ and *Pdgfra*$^{+}$*/Wnt2*$^{+}$*/Wnt5a*$^{+}$ appear spatially separated (albeit over a narrow distance range), where hypercapnic injury reduces the spatial separation of *Wnt2* versus Wnt5a RNA signals proximal to AT2 cells, we reason that hypercapnia disrupts the spatial Wnt code of the AT2 niche.

.

Discussion

We describe a mechanism by which hypercapnia, an inevitable consequence of a lung protective ventilation strategy, slows or prevents lung repair after injury. We found hypercapnia decreases AT2 cell progenitor activity by modulating the repertoire of Wnt signals in mesenchymal cells comprising the AT2 stem cell niche. Specifically, hypercapnia reduced expression of Wnt ligands that promote βcat signaling in AT2 cells, and simultaneously enhanced expression of Wnt ligands that inhibit βcat signaling. These changes affected the AT2 cell microenvironment, leading to reduced AT2 proliferation. Our results suggest that patho-physiological conditions that impact the AT2 niche, including hypercapnia, can disrupt signals from the mesenchyme required to restore the alveolar barrier function and lung homeostasis after injury (**Figure 9**).

Previous lineage tracing experiments showed that a subgroup of AT2 cells, while retaining their surfactant biosynthetic capacity, can act as facultative progenitors (19). Our experiments suggest that the proliferative capacity of AT2 cells is decreased by hypercapnia. In a 3D-organoid model, the inhibitory effects of hypercapnia on the proliferative capacity of AT2 cells are so severe that if the organoid incubation is started in hypercapnia equilibrated media, no organoids are formed. The decrease in AT2 proliferative capacity was also observed in lungs isolated from mice exposed to high CO_2 for 21 days. To identify signaling pathways responsible for the hypercapnia-mediated decrease in proliferative activity, we analyzed the transcriptomic signature elicited in AT2 cells isolated from mice breathing room air or high CO_2. We observed changes in the transcriptomic signature at 21, but not at 7 days of hypercapnia. At 21 days, hypercapnia decreased canonical AT2 markers, including *Sftpc* and genes involved in lipid metabolism (*Hmgcr, Fabp5*), as well as essential regulators of AT2-cell specification, such as *Etv5* and *Abca.* We also observed an increase in the expression of genes involved in cell adhesion, tissue remodeling and cytoskeleton reorganization. Together, these data suggest hypercapnia causes a loss of AT2 cell morphological as well as functional characteristics.

Accumulating evidence suggest that canonical Wnt signaling is essential for alveolar progenitor cells to undergo alveolar epithelial repair after injury (18, 19, 31). The ubiquitous Wnt/βcat target gene and negative feedback regulator *Axin2,* marks a sub-population of Wnt-responsive AT2 cells with progenitor characteristics (16, 19). Consistent with previous observations, we found that Wnt/βcat activity (evidenced by *Axin2* expression) is very

low in control AT2 cells. A recent publication suggested *Wnt5a*/WNT5A expressed by fibroblasts in close proximity to AT2 cells can induce canonical Wnt signaling, promote AT2 cell cycle entry and maintain the AT2 cell fate (19). While these activities are typically attributed to elevated βcat signaling, and WNT5A can promote βcat signaling in certain contexts (48), our data reinforce a model in which WNT5A limits βcat signaling in AT2 cells. We validated WNT-subtype functionality in primary AT2 cultures, showing that WNT5A limits, whereas WNT3A enhances βcat protein levels and signaling. Our results align with a recent lung organoid study showing that WNT5A and WNT5B ligands inhibit alveolar epithelial stem/progenitor expansion by impairing canonical Wnt signaling (38), and longstanding evidence that WNT5A limits βcat signals in lung and other tissues (49, 50). Our data are also consistent with evidence that the mesenchymal population that sustains the self-renewal and differentiation of AT2 stem cells is positive for *Wnt2 and other genes* (21).

Our results highlight the importance of methods that provide single-cell spatial resolution in studies of lung repair. Spatial transcriptomic approaches allowed us to localize these signals specifically to mesenchymal cells near AT2 cells. We found that freshly isolated PDGFRα$^+$ cells can be distinguished as 4-subtypes regarding *Wnt2/Wnt5a* expression: *Wnt2*$^+$, *Wnt5a*$^+$, *Wnt2*$^+$*/Wnt5a*$^+$ and *Wnt2/Wnt5a*-negative. These data also suggest AT2 niche cells (i.e., PDGFRα stromal cells) may be targets of pathological conditions like hypercapnia, where the spatial arrangement of distinct PDFGRα$^+$ stroma cell-subtypes may direct AT2 cell proliferative versus differentiative zones of the alveolus. Using RNA-FISH analysis, we found that *Wnt2*-expressing *Pdgfrα*$^+$ cells are spatially closer to *Sftpc*$^+$AT2 cells than *Wnt5*a-expressing cells. Together these data suggest that a more systematic evaluation of the major stromal derived Wnts may shed light on how individual AT2 cells are selected for activation.

Our results do not exclude pathogenic effects of hypercapnia on AT2 cells independently of the niche. Indeed, hypercapnia can inhibit proliferation of both lung epithelial (A549 human lung carcinoma) and fibroblast (N12) cell cultures (8). As the former is known to express WNT5A (51, 52), future studies will be required to distinguish whether the anti-proliferative effects of hypercapnia are due to WNT5A or other targets in these cells.

In summary, we demonstrate a fundamental effect of elevated CO_2 levels on alveolar epithelial cell behavior, which is regulated by Wnt signal modulation, which inhibits reparative AT2 progenitor cell function. These findings are of biological and clinical relevance as they pertain to patients with severe COVID-19 ARDS requiring mechanical ventilation. Inhibition of AT2 proliferation in hypercapnic patients prevents the sealing of the epithelial barrier, increasing lung flooding, ventilator dependency and mortality. We contend that the hypercapnia-mediated mechanisms we uncovered are of relevance to lung repair, worsening the outcome of mechanically ventilated patients.

Methods

Mouse strains and Cre recombinase induction. Animal work was conducted in accordance with the recommendations in the Guide for the Care and Use of Laboratory Animals and the National Institute of Health. All procedures were approved by the Northwestern University's Institutional Animal Care and Use Committee (Chicago, IL, USA; Animal Study Number: IS00010662). All strains including wildtype mice are bred and housed at a barrier- and pathogen-free facility at the Center for Comparative Medicine at Northwestern University. Animal experiments were performed on both male and female animals in all conditions, and animals were chosen at random from the cohort but not formally randomized. Adult (8 to 10 weeks old) C57BL/6J mice were obtained from the Jackson Laboratories (Strain Number: 000664) and were used as the wildtype strain. *Sftpc*^{CreERT2}:*R26R*^{EYFP} and *Axin2*$^{CreERT2\text{-}TdTom}$,*Ctnnbl*$^{fl(ex3)/+}$ (were kindly provided by Dr. Edward E. Morrisey, University of Pennsylvania) and their genotyping and characterization has been previously described (18, 45, 53).

For induction of estrogen-inducible Cre recombinase (Cre-ERT2) for conditional-tissue-specific conditional alleles *in vivo*, tamoxifen was dissolved in sterile corn oil (Millipore Sigma (T5648)) at 20 mg/ml concentration. Mice were injected intraperitoneally three times over the course of five days with 0.25 mg/g body weight to induce Cre-recombination of floxed alleles for lineage tracing in *Sftpc*^{CreERT2}*:R26R*^{EYFP}(18).

Mice were provided with food and water ad libitum, maintained on a 14-hour light/10-hour dark cycle. For high CO_2 exposure, mice were maintained at 10% CO_2 in a BioSpherix C-Shuttle Glove Box (BioSpherix) for up to 21 days as described previously (54). Control mice were maintained in the adjacent space under room air conditions. We have previously shown that mice exposed to high CO_2 had elevated $PaCO_2$ and higher bicarbonate values after 3 days of exposure reflecting renal compensation of the respiratory acidosis (55, 56). Treatment of mice with 10% CO_2 produces an arterial pCO_2 of ~77 mmHg which is not unusual in patients undergoing "permissive hypercapnia" mechanical ventilation and/or patients with COPD or in patients with a severe asthma attack (54). At the selected time points, mice were euthanized with Euthasol (pentobarbital sodium–phenytoin sodium) and the lungs were harvested.

Mouse AT2 cells isolation by flow cytometry. Tissue preparation for mouse AT2 isolation was performed as described (22, 23), with modifications. Multicolor flow cytometry and cell sorting were performed with an LSR Fortessa or BD FACSAria cell sorter using BD FACSDIVA software (BD Biosciences). Briefly, perfused lungs were treated with 50 U/ml dispase (Corning # 47743-724) and 0.25 mg/ml DNase (Sigma-Aldrich # D4513-1VL) and were subjected to manual dissection gently tearing and mincing the lung pieces. When required, single cell suspensions were enriched for epithelial cells using anti-EpCAM magnetic microbeads (Miltenyi Biotec # 130-105-958; Lot # 5210607845).

Lungs from wild-type, *Sftpc*^{CreERT2}:*R26R*^{EYFP} and *Axin2*$^{CreERT2\text{-}TdTomato}$ mice were processed into single-cell suspensions as indicated above. Wild-type AT2 cells: AT2 cells were sorted from the single-cell suspensions using antibody staining for CD31-PECy7, Clone 390 (eBioscience; #25-0311-81; Lot # 2313111), CD45-PECy7 Clone 30-F-11 (eBioscience # 25-0451-82; Lot #238036), and EpCAM-APC (eBioscience; # 17-5791-80; Lot #2202308). Wild-type AT2 cells $CD45^{-}CD31^{-}EpCAM^{+}$ cells were gated for MHCII-BUV395 Clone 2G9 (BDBioscience #743876; Lot # 02970248) and selected as $EPCAM^{Int}$ $MHCII^{high}$ as previously described (57) and showed in **Supplemental Figure 1**. *Sftpc*^{EYFP} - AT2 cells: following negative selection for CD31 and CD45, YFP^{+}-AT2 cells were isolated based on enhanced YFP (EYFP) fluorescence and sorted as indicated above and in **Supplemental Figure 1**. *Axin2*^{TdTom}- AT2 cells: following negative selection for CD31 and CD45, $Axin2^{+}$-AT2 cells were positively gated for TdTomato and EpCAM as indicated above and in **Supplemental Figure 4**. Compensation, analysis, and visualization of the flow cytometric data were performed using FlowJo software (FlowJo,L.L.C., 10.7.1). "Fluorescence minus one" controls were used to set up gates.

Alveolar Organoids and Hypercapnia Exposure. Clonal alveolar organoid assays were performed as described previously (13, 18). In brief, a mixture of AT2 cells (5 $x10^3$ AT2, YFP^{+}-AT2 or YFP^{+}- βcat ΔExon 3 and lung fibroblasts (5 x 10^4) in growth media containing the following: alpha-MEM media (Thermo Fisher #41061029) supplemented with 4.5 g/l D-glucose, 2mM L-glutamine, 10% FBS and 1% penicillin-streptomycin, 1% insulin/transferrin/selenium (Thermo Fisher #41400045), 0.002% Heparin, 0.25 ug/ml Amphotericin B (Millipore Sigma #A2942), 2.5 µg/ml ROCK inhibitor Y24632 (Selleckchem #S1049) was used for the assays. Lung fibroblasts for organoids assays were isolated from adult wild type mice and plated in DMEM supplemented

with 4.5 g/L D-glucose, 2mM L-glutamine, 10% FBS and 1% penicillin-streptomycin as previously described (16). Immediately before use cells were treated with mitomycin-C (Millipore Sigma #M4287) for 2 hours. Cells were then suspended in a 1:1 mixture of organoid growth media and growth factor-reduced, phenol-free Matrigel (Corning #356231). 100µl of the cell/media/matrigel mixture was then plated into individual 24 well cell culture inserts (Corning, #3470) and allowed to solidify at 37°C for 5 minutes. Organoid growth media was added into the bottom of the 24-well plate. After 5-7 days of culture, organoids were moved to normocapnic or hypercapnic conditions and grown for an additional 7-21 days.

We have previously described that the maximal effects of hypercapnia on signal transduction pathways is achieved at ~120 mmHg of CO_2 (8, 58), all the *in vitro* experiments in this publication were performed under those conditions. The desired CO_2 and pH levels were achieved by equilibrating the medium overnight in a humidified chamber (C-Chamber, BioSpherix, Lacona, NY). The atmosphere of the C-Chamber was controlled with a PRO CO_2 carbon dioxide controller (BioSpherix). In this chamber, cells were exposed to the desired pCO_2 while maintaining 21% O_2 balanced with N_2. Routinely, before CO_2 exposure, pH, pCO_2, and pO_2 levels in the medium were measured using a Nova Stat Profile Prime CCS (Critical Care System) (Nova Biomedical, Waltham, MA). Experiments began by replacing the culture medium with the CO_2-equilibrated medium and (59) incubating in the C-Chamber for the desired time. The normocapnia growth media consisted of alpha-MEM/Ham's F-12 medium/Tris base/MOPS base (3:1:0.25:0.25) containing 10% FBS, 100 U/mL penicillin, and 100 µg/mL streptomycin solution pH=7.4 as we previously described (54, 60). The buffering capacity of the medium was achieved by changing its initial pH with Tris and MOPS base to obtain a pH of 7.4 at the experimental CO_2 levels (pCO_2 of 40 or 120 mmHg).

The organoid media with or without treatment was changed every 48 hours. Organoids were imaged on a Nikon Ti^2 Widefield in brightfield and GFP channels. In some cases, at the end of the experiment organoids were fixed in 4% paraformaldehyde. Images were processed in Nikon Elements (5.11.00) and quantified using ImageJ/Fiji software for organoid diameter. Alveolar organoids are defined as a clonal colony with a minimum diameter of 50 microns. The following antibodies were used Podoplanin (PDPN, DSHB University of Iowa

#8.1.1; 1:40), SFTPC (Millipore; AB3786; Lot # 3845252; rabbit polyclonal antibody; 1:250) and imaging was performed in a Nikon Eclipse Ti confocal microscope.

Immunostaining of whole lung sections. After lungs were cleared of blood by perfusion with cold PBS via the right ventricle, they were inflated with 4% paraformaldehyde and allowed to fix overnight. Tissue was then dehydrated, paraffin embedded, and sectioned. Hematoxylin and eosin staining was performed to examine morphology. Immunohistochemistry was used to detect protein expression using the following antibodies on paraffin sections: SFTPC, and Ki67 Clone SolA15 (eBioscience #14-5698-8, rat monoclonal antibody; 1:100). Following PBS washes, fluorophore-conjugated secondary antibodies were prepared at 1:500 for 60 minutes in the dark at room temperature. Hoechst 33342 (Invitrogen #3570) was diluted 1:1,000 and applied for 15 minutes at room temperature following secondary antibody incubation. Coverslips and filters were mounted using ProLong Gold anti-fade solution. Images were obtained using Zeiss Axioplan epifluorescence. Cell counts were performed using ImageJ software (https://imagej.nih.gov/ij)

Isolation of mouse lung fibroblasts. Mesenchymal populations from whole lung were isolated from wildtype C57Bl/6 mice. Briefly, perfused lungs were inflated with digestion buffer containing 200 U/ml Collagenase (Millipore Sigma; Cat # C0130-500 mg); 4 U/ml Elastase (Worthington; Cat # LS002292), 0.25 mg/mL DNase (Sigma; Cat # D4513-1VL) and coarsely minced before processing in C-tubes (Miltenyi Biotec) with a GentleMACS dissociator (Miltenyi Biotec) according to the manufacturer's instructions. Homogenate was passed through 40-μm nylon filter to obtain a single-cell suspension and subjected to red blood cell lysis reagent (BD Pharm Lyse, BD Biosciences). Cells were subjected to negative selection using CD45 and CD31 magnetic microbeads (Miltenyi Biotec # 130-052-301; Lot #5220509667 and 130-097-418; Lot # 521101846) and live cells selected using Sytox Green (Invitrogen # 2420608). Fibroblasts cells were identified as $CD45^-$ $CD31^-$ $EPCAM^-$ $PDGFRA^+$ by flow cytometry as outlined in **Supplemental Figure 5** using PDGFRA antibody (eBioscience #12-1401-81; Lot #2124709).

Transcriptomic profiling via RNA-Seq. FACS-based isolation of AT2 cells or $PDGFR\alpha^+$ fibroblasts from wild type mice was performed at the indicated time points for each experiment as described above. The RNeasy

Plus Micro Kit (Qiagen, 74034) was used to isolate RNA and remove genomic DNA. RNA quality was assessed with the 4200 TapeStation System (Agilent Technologies). Samples with an RNA integrity number (RIN) lower than 7 were discarded. RNA-Seq libraries were prepared from 5 ng total RNA using the NEB Next RNA Ultra Kit (QIAGEN) with poly(A) enrichment. Libraries were quantified and assessed using the Qubit Fluorimeter (Invitrogen, Thermo Fisher Scientific) and the Agilent TapeStation 4200. Libraries were sequenced on the NextSeq 500 instrument (Illumina) at 75 bp length, single-end reads. The average reading depth across all experiments exceeded 6×10^6 per sample, and over 94% of the reads had a Q score above 30. Bioinformatics work was performed on "Genomics Nodes" using Northwestern High-Performance Computing Cluster, Quest (Northwestern IT and Research computing). Reads were demultiplexed using bcl2fastc (version 2.17.1.14). Quality was controlled with FastQC. Samples that did not pass half of the 12 assessed quality control (QC) statistics were eliminated. Then reads were trimmed and aligned to mm10 reference genome using TopHat2 aligner (version 2.1.0). Reads counts were associated with genes using the GenomicRanges (61). The downstream differential gene expression was conducted with edgeR R/Bioconductor packages (62, 63). Genes with less than 1 normalized counts from more than 3 samples were excluded from the analysis. Hierarchical clustering heatmaps were also performed for top 1,000 most differential expressed genes. Statistical significance was controlled at a *P*-value of 0.05 with False Discovery Rate (FDR) adjusting for multi-pairwise comparison. GO analysis was performed using GOrilla (64) on 2 unranked gene lists.

Quantitative real time PCR. RNA was isolated from primary AT2 cells or PDGFRα$^+$ fibroblasts or cultured fibroblast cell line (Mlg 2908-CCL-206; ATCC), and purified using RNeasy Plus Micro Kit before cDNA preparation with qScript cDNA synthesis kit (Quanta Bio, 95047). For qRT-PCR, IQ SybrGreen master mixes (Bio-Rad, 1708880) were used according to manufacturer's instructions. The following primers used are described in **Supplemental Table 1**. TaqMan qPCR was performed for Wnt2 using pre-designed TaqMan primer/probe sets (Life Technologies, Assay ID: Mm01156901) using Gapdh (Assay ID: Mm99999915_g1) following manufacturer's instruction. qPCR was performed in triplicate for each biological sample and fold enrichment was calculated from ΔCt values for each gene of interest, normalized to expression of housekeeping genes.

Immunoblotting. Protein content in cell lysates was quantified by Bradford assay. Equal amounts of proteins were resolved on polyacrylamide gels (SDS-PAGE). Proteins were transferred to a nitrocellulose membrane using a Trans-Blot-Turbo Transfer System (Bio-Rad). Incubation with specific primary antibodies was performed overnight at 4 °C. SFTPC was detected using Millipore; rabbit polyclonal antibody AB37086 (1:2500) and actin using a rabbit polyclonal antibody from Sigma-Aldrich (#2066; Lot # 018M4753V; 1:2000). HRP-tagged secondary antibodies (Bio-Rad, 1721011 and 1721019) were used in combination with Super-Signal ECL kit (Thermo Fisher) to develop blots using a LI-COR Fc Odyssey Imager and companion software Image Studio version 5.2. Blots were quantified by densitometry (ImageJ 1.46r; National Institutes of Health, Bethesda, MD).

Single Molecule mRNA Fluorescent in Situ Hybridization (RNA-FISH). Multiplex fluorescence *in situ* hybridization was performed using RNAscope (Advanced Cell Diagnostics (ACD), Newark, CA, USA). Mouse lungs were inflated to 15 cm H_2O and fixed with 4% paraformaldehyde (EMS, Hatfield, PA, USA) for 24 h. Lungs were paraffin embedded and 5 µm tissue sections were mounted on Superfrost Plus slides (Thermo Fisher Scientific, Waltham, MA, USA). Slides were baked for 1 h at 60°C, deparaffinized in xylene and dehydrated in 100% ethanol. Sections were treated with H_2O_2 (ACD# 32281) for 10 min at room temperature and then heated to mild boil (98–102°C) in 1× target retrieval reagent buffer (Advanced Cell Diagnostics, ACD) for 15 min. Protease Plus (ACD#32281) was applied to sections for 30 min at 40°C in a HybEZ Oven (ACD). Hybridization with target probes, pre-amplifier, amplifier, fluorescent labels, and wash buffer (ACD) was done according to manufacture' instructions for Multiplex Fluorescent Reagent Kit version 2 (#322809). Parallel sections were incubated with ACD positive and negative control probes. Sections were covered with ProLong Gold Antifade Mounting (Invitrogen). Mouse probes used were: *Wnt2*-C1 (#323601-C1), *Wnt5a*-C1 (#316791-C1), *Wnt5a*-C2 (#316791-C2), *Wnt5a*-C3 (#316791-C3), *PDGFRa*-C2 (480661-C2), *Sftpc*-C3 (#314101-C3), *Axin2*-C1 (#400331-C1), Mouse Negative Control #320871, Mouse Positive Control #320881, all from ACD. Opal fluorophores (Opal 520 #FP1487001KT; Opal 620 #FP1495001KT; Opal 690 #FP1497001KT) from Akoya (Perkin Elmer, Shelton, CT) were used at 1:1500 dilution in Multiplex TSA buffer (ACD#322809). Images were captured on a Nikon A1R confocal microscope (Tokyo, Japan) with ×20 and ×40 objectives, followed by uniform processing and pseudo-coloring in Fiji (https://imagej.net/Fiji).

For cytospins freshly isolated mouse lung PDGFRα$^+$ fibroblasts were centrifuged at 300g for 10 min at 4^{o}C and resuspended in PBS. Multiple replicates of 20,000 cells in 150μl volume were loaded to Cytofunnels (Shandon) and applied to Superfrost Plus charged slides (Fisher) by centrifugation in Cytospin 3 centrifuge (Thermo-Shandon) at 1000rpm for 5 min. Adherent cells were fixed, dehydrated, stored, rehydrated, and pretreated with hydrogen peroxide (ACD322381) and protease III (ACD 322340) according to sample preparation method (ACD RNAscope Multiplex Fluorescent v2 Assay, Tech Note MK 50 010) for cultured adherent cells, ACD RNAscope Multiplex Fluorescent v2 Assay, Tech Note MK 50 010.")

Spatial analysis of the mouse lung. To assess spatial proximity of *Wnt2*, *Wnt5a* and *Pdgfra* mRNA signals to *Sftpc*-positive AT2 cells, quantification was performed using Nikon NIS-Elements software version 5.30.02 using the General Analysis module, NearstObjDist algorithm. For each RNA-FISH probe, thresholding allows us to distinguish specific signal over background, generating a binary layer based on the size and intensity of objects (a single probe detected by NIS-Element algorithm) using Bright Spot Detection thresholding (specifically the Bright, Clustered detection method). General diameter and contrast were then adjusted for each object then converted to "spots" to produce a 3-pixel, centroid of objects. This converts the RNA-FISH signal into objects (circle/spot) based on signal density, so distances can be measured between spot centers. The smallest distance a given "spot" of channel/color (e.g., *Pdgfra*$^+$ spot) is from the other two channel/color "spots" (e.g., *Sftpc*$^+$ spot or *Wnt2*$^+$ spot) is measured for all image spots. Mean shortest distance measurements were quantified and plotted in Prism.

Identification of subtypes of Pdgfra$^+$ *fibroblast following isolation and cytospin.* Following fluorescence in situ RNA hybridization protocol, mouse probes for *Pdgfra*, *Wnt2*, and *Wnt5a* were used to distinguish subtypes of *Pdgfra* fibroblasts. Signals of *Pdgfra*$^+$ and *Wnts* were captured by Bright Spot Detection thresholding using Nikon NIS-Elements, with similar methodology as discussed previously. *Pdgfra*$^+$ objects were then dilated by 5 μm and combined with DAPI signal to form new binaries – a representation of *Pdgfra*$^+$ fibroblasts. To capture plausible RNA signals within "*Pdgfra*$^+$ fibroblasts," simple Boolean operator expressions (using the Combine

function of General Analysis) were used to identify subpopulations of *Pdgfra*$^{+}$ cells overlapping with *Wnt* binary layer(s) which was also dilated by 4 μm for detection.

β-catenin/TCF Reporter Assay. A549 cells (1.5x10^{5} cell/well) were transfected with Super8-TOPflash (containing 8 TCF-consensus binding sites) or 1 μg of Super8-FOPflash (8 mutant TCF-binding sites) reporter plasmids (kindly provided by Randall Moon, University of Washington, Seattle) using Lipofectamine 2000 (Invitrogen); a thymidine kinase-Renilla plasmid (0.1 μg) was also included to normalize luciferase values to the efficiency of transfection as we previously described (17). After 4 hours of transfection, media was replaced, and cells were incubated overnight under normocapnic or hypercapnic conditions. The next morning rWnt3 (50ng/ml) or rWnt5a (50ng/ml) was added to the media and cells were incubated for another 24 hours. At the end of the incubation, A549 cells were solubilized using the Dual-Luciferase Assay Kit (Promega), and luciferase activity was quantified using a microplate dual-injector luminometer (Veritas) according to manufacturer's instructions. Briefly, cells in each well of a 6 well plate were incubated on ice with 250uL of a 1x passive lysis buffer for 15 minutes followed by scraping to lift adherent cells. 20 μl of cell lysate was mixed with 100 μL of supplied Luciferase Assay Reagent II and firefly luciferase was measured.

Measurement of β-catenin signaling pool. AT2 cells were isolated from rat lungs as described (17, 65) . 3x10^{6} AT2 cells were plated to 100mm (low density), 60mm (medium density), and 35mm (high density) culture dishes and immediately infected with 20 pfu/cell adenovirus (Vector Biolabs, 10^{10}–10^{12} pfu/ml).): Ad-CMV-GFP, Ad-Wnt3a, and Ad-Wnt5a. Infection efficiency of (>90%) was confirmed by visualizing GFP expression in living cells. Cells were lysed after 72 hours as described (17). Protein lysates were processed for GST-ICAT pulldown as described (43). Briefly, 100 μg of lysate was saved as input fraction. 1000 μg of lysate was combined with 50 μl of a 50:50 slurry of pre-washed glutathione-sepharose beads (GE 4B), and 20 μg of GST-ICAT and tumbled at 4^{o}C for 2 hours. Samples were centrifuged at 10,000 rpm for 1 minute to pellet beads, and a 5 μl aliquot of supernatant was collected as the unbound fraction. Beads were washed with 0.1% triton buffer and centrifuged three times, and the final pellet resuspended in 35 μl 2X SDS loading buffer as bound pulldown fraction. Protein lysates were run on 6% acrylamide gel and transferred to nitrocellulose for immunoblotting as described above. Primary antibodies: mouse anti-ABC Clone 8E7 (Millipore #05-665, Lot # 2275597) 1:1000,

mouse anti-β-cat Clone 14 (BD #610154; Lot #1085870) 1:1000 or 1:5000, mouse anti-E-cadherin Clone 36 (BD #610182; Lot #4353669) 1:1000 and rabbit-anti-GAPDH (Santa Cruz #sc-25778; Lot #D1613) 1:1000.

Data and materials availability. All data needed to evaluate the conclusions in the paper are present in the paper and/or the Supplementary Materials. The RNA-Seq data sets are available at in the NCBI's Gene Expression Omnibus (GEO) database #GSE139426 Room Air/Hypercapnia AT2 cells; for PDGFRα^{+}-fibroblasts Room Air/Hypercapnia the record is process.

Statistics. Analyses of significance were performed using GraphPad Prism (v.8.4.2) software. A p value ≤0.05 was considered statistically significant. A standard two-tailed unpaired Student's t-test was used for statistical analysis of two groups. One-way ANOVA, followed by analysis-specific post-tests, was carried out when more than two variables were compared. Unless stated otherwise data are presented mean ± S.D. overlaid with individual data points representing replicates.

Study approval. Animal work was conducted in accordance with the recommendations in the Guide for the Care and Use of Laboratory Animals and the National Institute of Health. All procedures were approved by the Northwestern University's Institutional Animal Care and Use Committee (Chicago, IL, USA; Animal Study Number: IS00010662). All strains including wildtype mice are bred and housed at a barrier- and pathogen-free facility at the Center for Comparative Medicine at Northwestern University

Authors contributions

LAD, LCW, CJG, and JIS conceived and designed the research. LAD, LCW, NDM, HH, PLB, DC, ASF, AW, MMH, HAV, MS, SMCM, CER performed and analyzed the experiments. LAD, LCW, NDM, HH, PLB, AVM and CJG analyzed the experimental data. ZR and AVM performed the bioinformatic analysis. LAD, GRSB, CJG, JIS wrote the manuscript. All authors provided edits and feedback on the manuscript.

Acknowledgements

This study was supported by the following grants. J.IS. was supported by NIH grants R01HL147070, P01AG049665, 5T32HL076139 and P01HL154998. L.A.D was supported by NIH grants P01AG049665 and P01HL154998. M.S by NIH grant R01HL147070. CJG by R01HL134800, HL163611, ARO073270 and GM129312. G.R.S.B. was supported by NIH grants U19AI35964, P01AG049665, P01AG04966506S1, R01HL147575 and Veterans Affairs grant I01CX001777. A.V.M. was supported by NIH awards U19AI35964, P01AG049665, R21AG075423, R01HL158139, R01HL153312, P01HL154998. Imaging work was performed at the Northwestern University Center for Advanced Microscopy generously supported by NCI CCSG P30CA060553. Histology services were provided by the Northwestern University Mouse Histology and Phenotyping Laboratory which is supported by NCI P30-CA060553. Northwestern University Flow Cytometry Core Facility is supported by NCI Cancer Center Support Grant P01AG049665.

This research was supported in part through the computational resources and staff contributions provided by the Genomics Compute Cluster, which is jointly supported by the Feinberg School of Medicine, the Center for Genetic Medicine, and Feinberg's Department of Biochemistry and Molecular Genetics, the Office of the Provost, the Office for Research and Northwestern Information Technology. The Genomics Compute Cluster is part of Quest, Northwestern University's high-performance computing facility, with the purpose to advance research in genomics.

The authors would like to thank Yair Romero Lopez, Fei Chen and Ziyan Lu for their technical support.

References

1. Dada LA, and Sznajder JI. Mechanisms of pulmonary edema clearance during acute hypoxemic respiratory failure: role of the Na,K-ATPase. *Crit Care Med.* 2003;31(4 Suppl):S248-52.
2. Sznajder JI. Alveolar Edema Must Be Cleared for the Acute Respiratory Distress Syndrome Patient to Survive. *Am J Respir Crit Care Med.* 2001;163:1293-4.
3. Nalbandian A, et al. Post-acute COVID-19 syndrome. *Nat Med.* 2021;27(4):601-15.
4. Morales-Quinteros L, et al. The role of hypercapnia in acute respiratory failure. *Intensive Care Med Exp.* 2019;7(Suppl 1):39.
5. Barnes T, et al. Re-examining Permissive Hypercapnia in ARDS: A Narrative Review. *Chest.* 2018;154(1):185-95.
6. Shigemura M, et al. Effects of hypercapnia on the lung. *J Physiol.* 2017.
7. Vadasz I, et al. Hypercapnia: a nonpermissive environment for the lung. *Am J Respir Cell Mol Biol.* 2012;46(4):417-21.
8. Vohwinkel CU, et al. Elevated CO(2) levels cause mitochondrial dysfunction and impair cell proliferation. *J Biol Chem.* 2011;286(43):37067-76.
9. Bharat A, et al. Pleural Hypercarbia After Lung Surgery Is Associated With Persistent Alveolopleural Fistulae. *Chest.* 2016;149(1):220-7.
10. Bharat A, et al. High CO2 levels impair lung wound healing. *Am J Respir Cell Mol Biol* 2020;63(2):244-54.
11. Desai TJ, et al. Alveolar progenitor and stem cells in lung development, renewal and cancer. *Nature.* 2014;507(7491):190-4.
12. Aspal M, and Zemans RL. Mechanisms of ATII-to-ATI Cell Differentiation during Lung Regeneration. *Int J Mol Sci.* 2020;21(9).
13. Barkauskas CE, et al. Type 2 alveolar cells are stem cells in adult lung. *J Clin Invest.* 2013;123(7):3025-36.
14. Hogan BL, et al. Repair and regeneration of the respiratory system: complexity, plasticity, and mechanisms of lung stem cell function. *Cell Stem Cell.* 2014;15(2):123-38.
15. Basil MC, and Morrisey EE. Lung regeneration: a tale of mice and men. *Semin Cell Dev Biol.* 2019.

16. Zacharias WJ, et al. Regeneration of the lung alveolus by an evolutionarily conserved epithelial progenitor. *Nature.* 2018;555(7695):251-5.

17. Flozak AS, et al. Beta-catenin/T-cell factor signaling is activated during lung injury and promotes the survival and migration of alveolar epithelial cells. *J Biol Chem.* 2010;285(5):3157-67.

18. Frank DB, et al. Emergence of a Wave of Wnt Signaling that Regulates Lung Alveologenesis by Controlling Epithelial Self-Renewal and Differentiation. *Cell Rep.* 2016;17(9):2312-25.

19. Nabhan AN, et al. Single-cell Wnt signaling niches maintain stemness of alveolar type 2 cells. *Science.* 2018;359(6380):1118-23.

20. Lee JH, et al. Anatomically and Functionally Distinct Lung Mesenchymal Populations Marked by Lgr5 and Lgr6. *Cell.* 2017;170(6):1149-63.e12.

21. Zepp JA, et al. Distinct Mesenchymal Lineages and Niches Promote Epithelial Self-Renewal and Myofibrogenesis in the Lung. *Cell.* 2017;170(6):1134-48 e10.

22. Magnani ND, et al. HIF and HOIL-1L-mediated PKCzeta degradation stabilizes plasma membrane Na,K-ATPase to protect against hypoxia-induced lung injury. *Proc Natl Acad Sci U S A.* 2017;114(47):E10178-e86.

23. Brazee PL, et al. Linear ubiquitin assembly complex regulates lung epithelial–driven responses during influenza infection. *J Clin Invest.* 2020;130(3):1301-14.

24. Misharin AV, et al. Nonclassical Ly6C(-) monocytes drive the development of inflammatory arthritis in mice. *Cell Rep.* 2014;9(2):591-604.

25. Reyfman PA, et al. Single-Cell Transcriptomic Analysis of Human Lung Provides Insights into the Pathobiology of Pulmonary Fibrosis. *Am J Respir Crit Care Med.* 2018.

26. Choi J, et al. Inflammatory Signals Induce AT2 Cell-Derived Damage-Associated Transient Progenitors that Mediate Alveolar Regeneration. *Cell Stem Cell.* 2020;27(3):366-82.e7.

27. Zhang Z, et al. Transcription factor Etv5 is essential for the maintenance of alveolar type II cells. *Proc Natl Acad Sci U S A.* 2017;114(15):3903-8.

28. Treutlein B, et al. Reconstructing lineage hierarchies of the distal lung epithelium using single-cell RNA-seq. *Nature.* 2014;509(7500):371-5.

29. Dorry SJ, et al. FGFR2 Is Required for AEC2 Homeostasis and Survival after Bleomycin-induced Lung Injury. *Am J Respir Cell Mol Biol.* 2020;62(5):608-21.

30. Balasooriya GI, et al. FGFR2 is required for airway basal cell self-renewal and terminal differentiation. *Development.* 2017;144(9):1600-6.

31. Raslan AA, and Yoon JK. WNT signaling in lung repair and regeneration. *Molecules and cells.* 2020;43(9):774.

32. Larraguibel J, et al. Wnt ligand-dependent activation of the negative feedback regulator Nkd1. *Mol Biol Cell.* 2015;26(12):2375-84.

33. Bänziger C, et al. Wntless, a conserved membrane protein dedicated to the secretion of Wnt proteins from signaling cells. *Cell.* 2006;125(3):509-22.

34. Li CM, et al. CTNNB1 mutations and overexpression of Wnt/beta-catenin target genes in WT1-mutant Wilms' tumors. *Am J Pathol.* 2004;165(6):1943-53.

35. Jho E-h, et al. Wnt/β-catenin/Tcf signaling induces the transcription of Axin2, a negative regulator of the signaling pathway. *Mol Cell Biol.* 2002;22(4):1172-83.

36. Shigemura M, et al. Elevated CO2 regulates the Wnt signaling pathway in mammals, Drosophila melanogaster and Caenorhabditis elegans. *Sci Rep.* 2019;9(1):18251.

37. Baarsma H, and Königshoff M. 'WNT-er is coming': WNT signalling in chronic lung diseases. *Thorax.* 2017;72(8):746-59.

38. Wu X, et al. Mesenchymal WNT-5A/5B Signaling Represses Lung Alveolar Epithelial Progenitors. *Cells.* 2019;8(10).

39. Najdi R, et al. A uniform human Wnt expression library reveals a shared secretory pathway and unique signaling activities. *Differentiation.* 2012;84(2):203-13.

40. Miller MF, et al. Wnt ligands signal in a cooperative manner to promote foregut organogenesis. *Proc Natl Acad Sci U S A.* 2012;109(38):15348-53.

41. Welch LC, et al. Extracellular signal-regulated kinase (ERK) participates in the hypercapnia-induced Na,K-ATPase downregulation. *FEBS Lett.* 2010;584(18):3985-9.

42. Rieger ME, et al. p300/beta-Catenin Interactions Regulate Adult Progenitor Cell Differentiation Downstream of WNT5a/Protein Kinase C (PKC). *J Biol Chem.* 2016;291(12):6569-82.

43. Flozak AS, et al. A Simple Method to Assess Abundance of the β-Catenin Signaling Pool in Cells. *Methods Mol Biol.* 2016;1481:49-60.

44. Harwood AJ. Regulation of GSK-3: a cellular multiprocessor. *Cell.* 2001;105(7):821-4.

45. Harada N, et al. Intestinal polyposis in mice with a dominant stable mutation of the beta-catenin gene. *EMBO J.* 1999;18(21):5931-42.

46. Kramer N, et al. Autocrine WNT2 signaling in fibroblasts promotes colorectal cancer progression. *Oncogene.* 2017;36(39):5460-72.

47. Jung YS, et al. Wnt2 complements Wnt/β-catenin signaling in colorectal cancer. *Oncotarget.* 2015;6(35):37257-68.

48. van Amerongen R, et al. Wnt5a can both activate and repress Wnt/β-catenin signaling during mouse embryonic development. *Dev Biol.* 2012;369(1):101-14.

49. Baarsma HA, et al. Noncanonical WNT-5A signaling impairs endogenous lung repair in COPD. *J Exp Med.* 2017;214(1):143-63.

50. Steinhart Z, and Angers S. Wnt signaling in development and tissue homeostasis. *Development.* 2018;145(11):dev146589.

51. Shojima K, et al. Wnt5a promotes cancer cell invasion and proliferation by receptor-mediated endocytosis-dependent and-independent mechanisms, respectively. *Scientific reports.* 2015;5(1):1-12.

52. Wang B, et al. Wnt5a promotes epithelial-to-mesenchymal transition and metastasis in non-small-cell lung cancer. *Bioscience reports.* 2017;37(6).

53. Chapman HA, et al. Integrin alpha6beta4 identifies an adult distal lung epithelial population with regenerative potential in mice. *J Clin Invest.* 2011;121(7):2855-62.

54. Shigemura M, et al. Hypercapnia increases airway smooth muscle contractility via caspase-7-mediated miR-133a-RhoA signaling. *Sci Transl Med.* 2018;10(457).

55. Gates KL, et al. Hypercapnia impairs lung neutrophil function and increases mortality in murine pseudomonas pneumonia. *Am J Respir Cell Mol Biol.* 2013;49(5):821-8.

56. Jaitovich A, et al. High CO2 levels cause skeletal muscle atrophy via AMP-activated kinase (AMPK), FoxO3a protein, and muscle-specific Ring finger protein 1 (MuRF1). *J Biol Chem.* 2015;290(14):9183-94.

57. Hasegawa K, et al. Fraction of MHCII and EpCAM expression characterizes distal lung epithelial cells for alveolar type 2 cell isolation. *Respir Res.* 2017;18(1):150.

58. Briva A, et al. High CO(2) Levels Impair Alveolar Epithelial Function Independently of pH. *PLoS ONE.* 2007;2(11):e1238.

59. Shoshani L, et al. The polarized expression of Na+,K+-ATPase in epithelia depends on the association between beta-subunits located in neighboring cells. *Mol Biol Cell.* 2005;16(3):1071-81.

60. Vadasz I, et al. AMP-activated protein kinase regulates CO2-induced alveolar epithelial dysfunction in rats and human cells by promoting Na,K-ATPase endocytosis. *J Clin Invest.* 2008;118(2):752-62.

61. Lawrence M, et al. Software for computing and annotating genomic ranges. *PLoS Comput Biol.* 2013;9(8):e1003118.

62. Robinson MD, et al. edgeR: a Bioconductor package for differential expression analysis of digital gene expression data. *Bioinformatics.* 2010;26(1):139-40.

63. McCarthy DJ, et al. Differential expression analysis of multifactor RNA-Seq experiments with respect to biological variation. *Nucleic Acids Res.* 2012;40(10):4288-97.

64. Eden E, et al. GOrilla: a tool for discovery and visualization of enriched GO terms in ranked gene lists. *BMC Bioinformatics.* 2009;10:48.

65. Dada LA, et al. High CO2 Leads to Na,K-ATPase Endocytosis via c-Jun Amino-Terminal Kinase-Induced LMO7b Phosphorylation. *Mol Cell Biol.* 2015;35(23):3962-73.

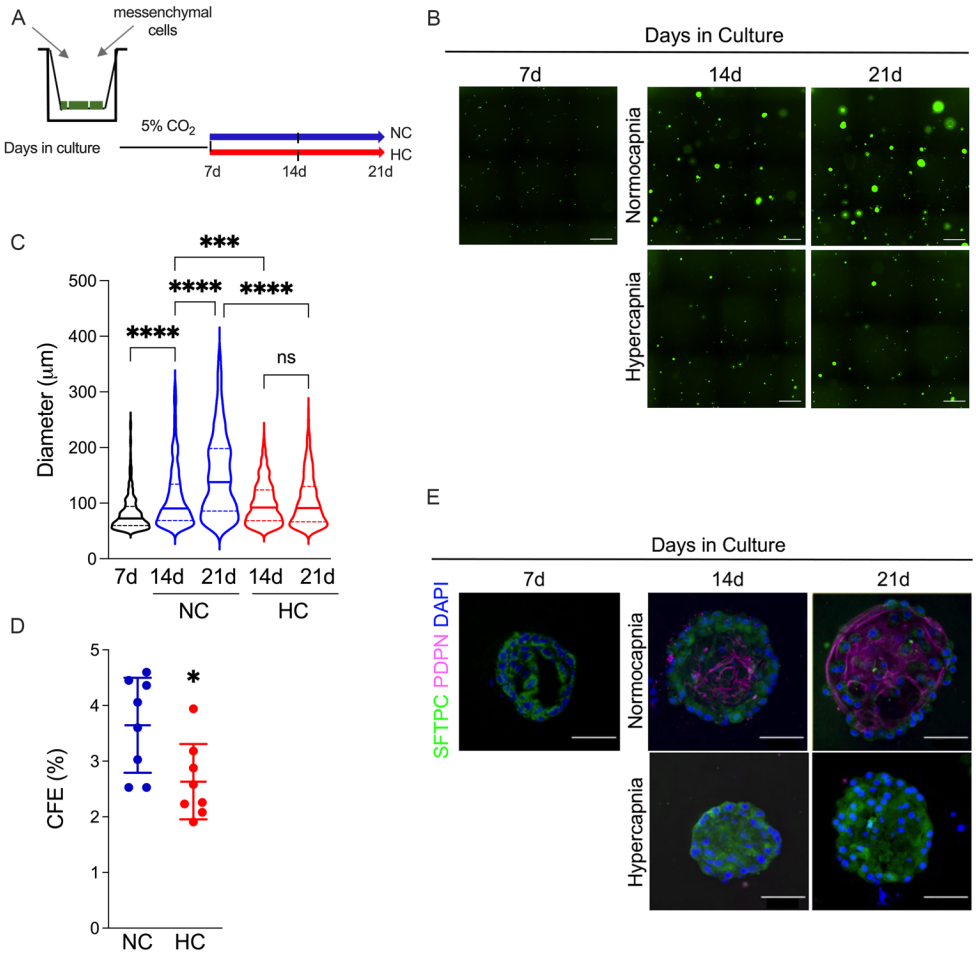

Figure 1. Hypercapnia limits AT2 cell proliferation in 3D culture organoids. (**A**) Schematic of experiments designed to co-culture AT2 cells isolated from *Sftp*^{CreERT2}*:R26R*^{EYFP} mice (*Sftpc*^{EYFP}-AT2) and wild-type mesenchymal cells. Alveolar organoids were switched to normocapnia (5% CO_2; NC) or hypercapnia (20% CO_2; HC) media on day 7 and cultured until day 21. (**B**) Representative images of organoid cultures in normocapnia or hypercapnia. Scale bars: 500 μm (**C**) Graph depicts the inhibitory effect of hypercapnia on organoid size. Median with interquartile range. n=8. (**D**) Graph depicts the effect of hypercapnia exposure for 21 days on colony forming efficiency (CFE) n=8. (**E**) Immunofluorescence analysis of SFTPC (AT2 marker) and Podoplanin (AT1 marker) revealed a reduction in AT2 cell proliferation in organoids exposed to hypercapnia for 14 days relative to normocapnia. Nuclear DNA is stained with DAPI. Scale bars: 50 μm. (C) ANOVA plus Sidak's multiple comparisons test and (D) Student's *t*-test. *P<0.05; ** P<0.01, ****P<0.0001.

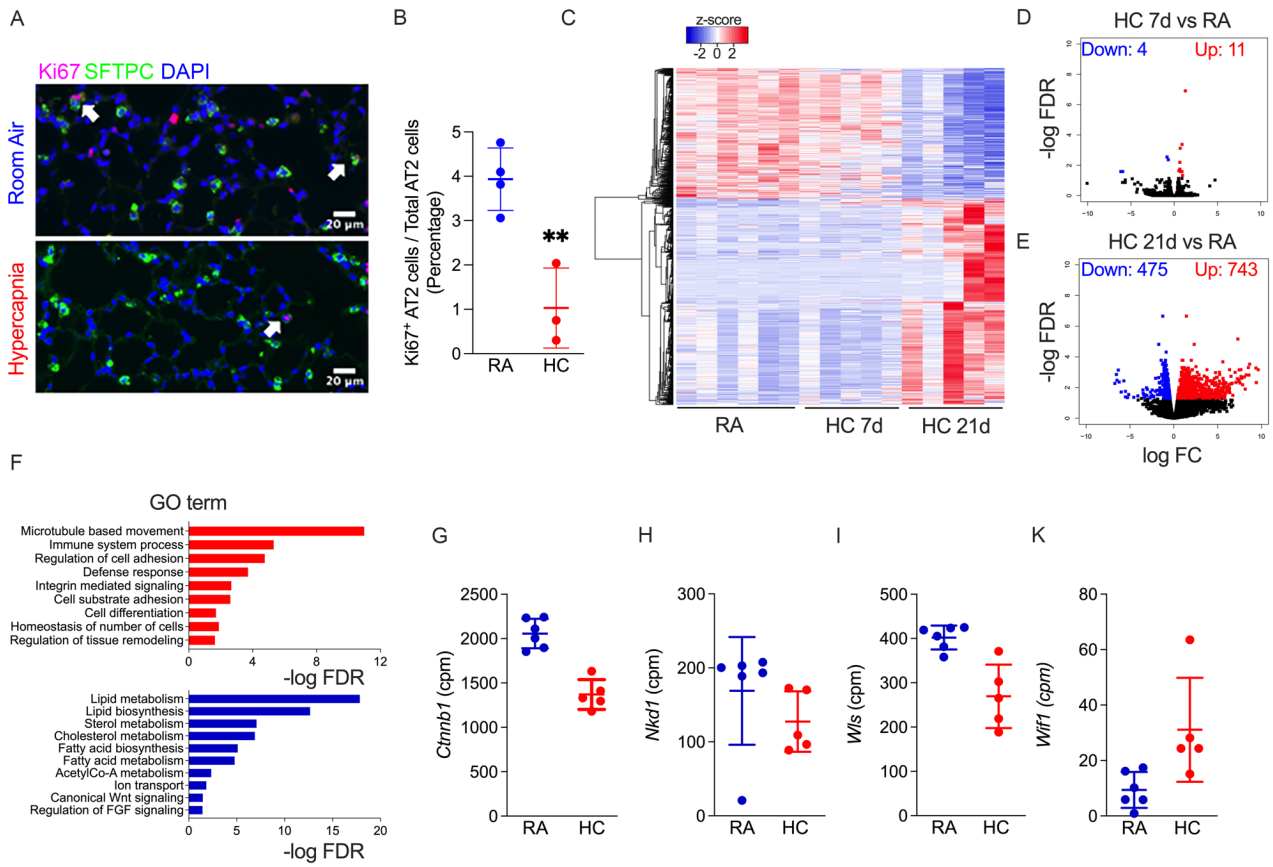

Figure 2. **Transcriptomic analysis of isolated AT2 cells reveals inhibition of βcat signaling during hypercapnia. (A)** Hypercapnia decreases the number of cells expressing Ki67 in the alveolar region of the adult mouse lung exposed to room air (RA) or 10% CO_2 (HC) for 21 days, as revealed by immunofluorescence. White arrows indicate SPTPC$^+$-Ki67$^+$ AT2 cells. Scale bars: 20 μm. **(B)** Graph depicting the inhibitory effect of hypercapnia exposure for 21 days on proliferation. RA n=4 and HC n=3 mice. Student's *t*-test. ***P*<0.01. **(C-F)** Bulk RNASeq was performed on flow cytometry sorted AT2 cells from mice breathing RA (n=6) or exposed to HC. Heatmap shows clustering of differentially expressed genes (FDR *q*< 0.05) in AT2 cells after 7 (n=5) or 21 (n=5) days of hypercapnia exposure. **(D and E)** Volcano plots. **(F)** GO biological processes. **(G-J)** Expression of selected DEG (FDR *q*< 0.05) regulated by hypercapnia involved in the Wnt/βcat pathway. ***P*<0.01.

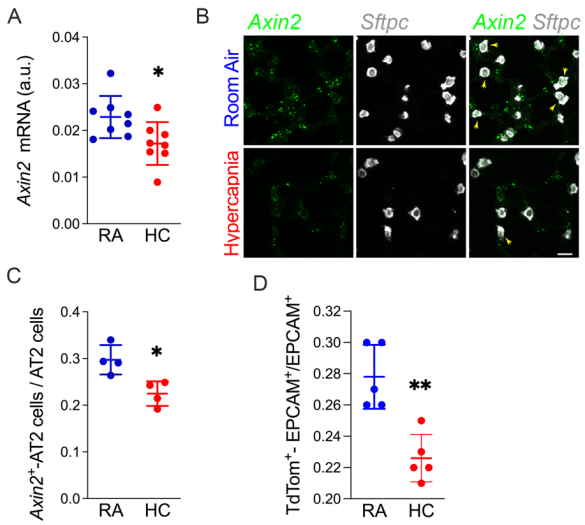

Figure 3. Hypercapnia decreases Wnt/βcat signaling in AT2 cells. AT2 cells were isolated from mice exposed to room air (RA) or 10% CO_2 (HC) for 21 days. (**A**) mRNA was isolated, and RT-qPCR was performed. n=8 mice. (**B and C**) *In situ* RNA hybridization showing decreased number of *Axin2*$^{+}$-AT2 cells in mice exposed to HC. In (B) yellow arrows indicate *Sftpc*$^{+}$-*Axin2*$^{+}$ AT2 cells. Scale bars: 10μm. n=4 mice. (**D**) Number of lineage-labeled AT2 cells from *Axin2*$^{CreERT2\text{-}TdTom}$ mice determined by flow cytometry. n=5 mice. Graph shows data from one of three independent experiments. Student's *t*-test. *p<0.05; **p<0.01.

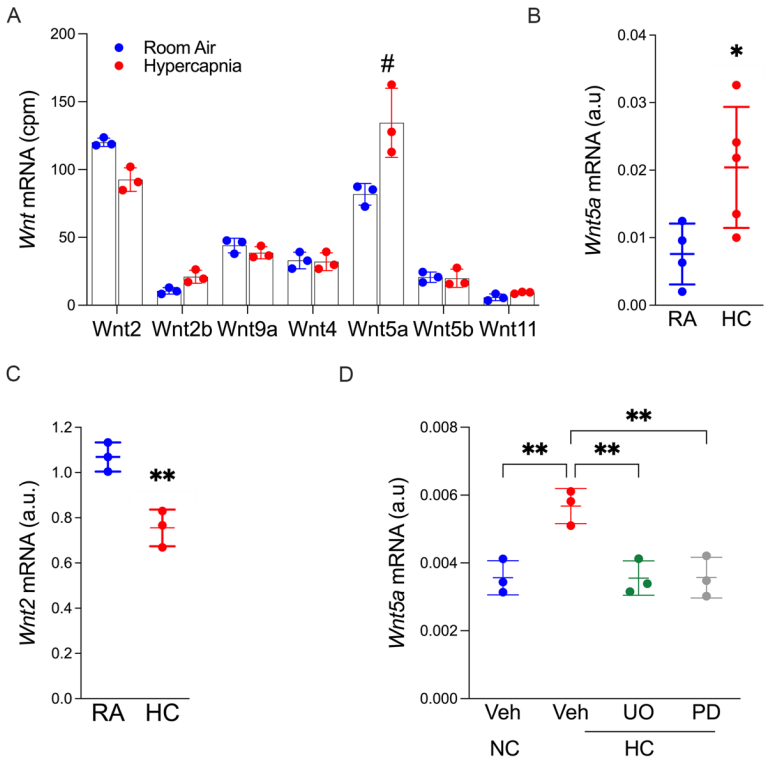

Figure 4. Hypercapnia increases *Wnt5a* expression in PDGFRα^{+} fibroblasts. Lung PDGFRα^{+} fibroblasts were isolated via flow cytometry cell sorting from mice breathing room air (RA) or exposed to 10% CO_2 (HC) for 10 days. **(A)** Expression of Wnt genes in PDGFRα^{+} fibroblasts as analyzed by population RNA-Seq. n=3, with cells isolated from 3 mice in each replicate. # Indicates DEG (FDR q< 0.05). (**B, C,** and **C**) mRNA was isolated, and RT-qPCR was performed. (**B**) *Wnt5a* (n=4) and (**C**) *Wnt2* (n=3). (**D**) MLg2908 mouse lung fibroblast cells were preincubated in the presence or absence of UO126 (10 μM) or PD98050 (10 μM) for 90 min and exposed to media equilibrated to NC (5% CO_2) or HC (20% CO_2) for 24h. n=3. (B-C) Student's *t*-test and (D) ANOVA plus Sidak's multiple comparisons test. *P<0.05; ** P<0.01.

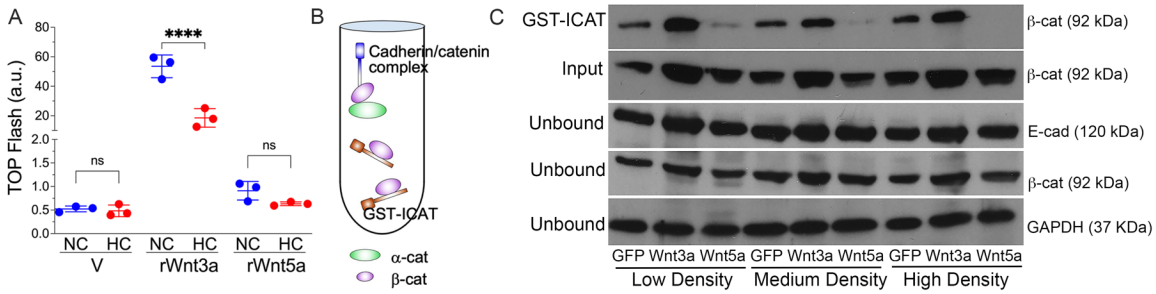

Figure 5. WNT5A reduces βcat signaling in alveolar epithelial cells. (**A**) βcat-transcriptional activity was measured using the established, T cell-factor (TCF) Optimal luciferase-based Promoter (TOPFlash). A549 cells were transiently transfected with the reporter plasmid for 24 h, and then stimulated with recombinant Wnts for another 16 h. Cell lysates, normalized to equal protein concentrations, were assayed for luciferase activity. V=Vehicle. n=3 independent experiments run in duplicate. (**B**) Schematic for assay to quantify the cadherin-free signaling pool of βcat in cell lysates via GST-ICAT (Inhibitor of Catenin and TCF) affinity precipitation as described in the Methods section. ICAT (brown protein) is an 81 amino acid polypeptide that binds the central armadillo-repeat region of βcat (purple) and can be used to quantify the Wnt-stabilized pool of βcat. Cadherin (blue) and α-catenin (green) also shown. (**C**) Immunoblot from rat AT2 cells plated at different densities and infected with adenoviruses coding for GFP, WNT3A-IRES-GFP or WNT5A-IRES-GFP and subjected to GST-ICAT affinity precipitation as in B. Input lysates and post-affinity precipitation (unbound lysates) are shown as controls. Note that across all cell plating conditions, WNT3A increases whereas WNT5A inhibits the GST-ICAT-bound (i.e., signal pool) of βcat. ****P<0.0001; ns= not significant. One way ANOVA with Sidak's post-comparison test.

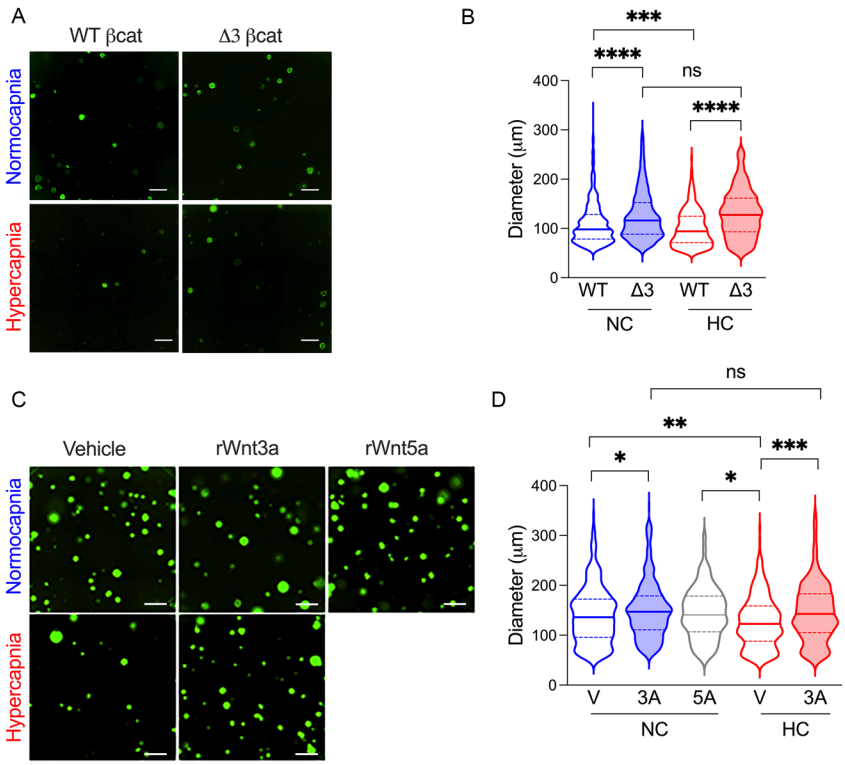

Figure 6. Activation of βcat signaling rescues AT2-proliferative capacity during hypercapnia. (**A**) Representative fluorescent images of typical day 21 organoid cultures of AT2 isolated from *Sftp*^{CreERT2}*:Ctnnb1*$^{wt/wt}$*:R26R*^{EYFP} mice (WTβcat) or *Sftp*^{CreERT2}*:Ctnnb1*^{flExon3fl}*:R26R*^{EYFP} (Δ3βcat). Organoids were cultured in NC or HC as described in Figure 1. Scale bars: 500μm. (**B**) Graph depicts effect of WTβcat vs Δ3βcat expression on Normocapnia (NC) and Hypercapnia (HC) organoid size. n=4 mice of each strain in 2 independent experiments. (**C**) Representative fluorescent images of typical day 21 organoid cultures of AT2 cells isolated from *Sftp*^{CreERT2}*:R26R*^{EYFP} mice treated with rWNT3A (50 ng/ml, 3a) or rWNT5A (50 ng/ml, 5a) starting 24h after switching media to NC or HC. Scale bars: 500 μm. (**D**) Graph depicts effect of added rWNT5A and rWNT3A on organoid size. n=4 mice of each strain in 3 independent experiments. Data are shown as median with interquartile range. *P<0.05; ** P<0.01***P <0.001; ****P <0.0001; ns=not significant. One way ANOVA with Sidak's post-comparison test.

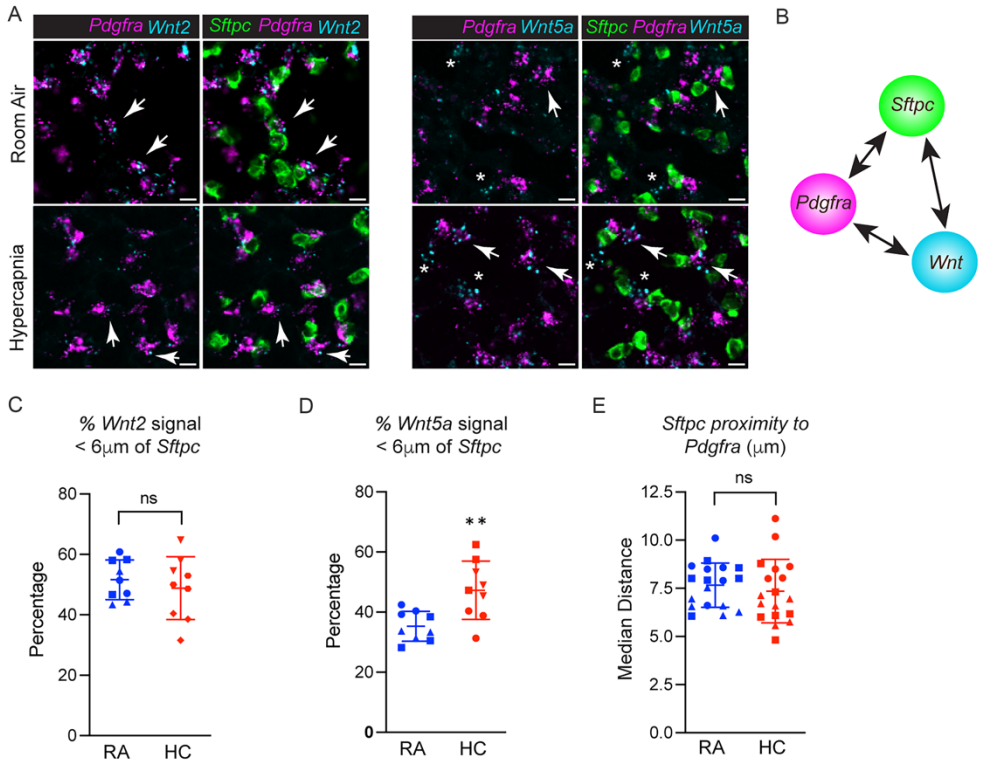

Figure 7. *Pdgfra*$^{+}$ *Wnt2*-expressing fibroblasts are spatially closer to AT2 cells than *Wnt5a*-expressing fibroblasts. (A) Confocal images of *Pdgfra, Sftpc, Wnt2* and *Wnt5a* mRNA signal in lung tissue from wild-type mice exposed to room air (RA) or hypercapnia (HC) for 10 days. RNA-FISH signal intensity converted to object spots to measure shortest distance between signals. White arrows indicate cells co-expressing signals. Scale bars:10μm. (**B**) Schematic of spatial distance mapping algorithm. See Methods for details. (**C** and **D**) Graphical representation of the percentage of *Wnt2* or *Wnt5a* spots from *Sftpc* mean signal, respectively. n=3 (each point consists of three mice), 3 fields of view/mouse with more than 1500 measurements per condition. Student's *t*-test. ***P*<0.01. (**E**) Graph shows that hypercapnia does not alter the median distance between *Pdfgra*$^{+}$ and *Sftpc* signals.

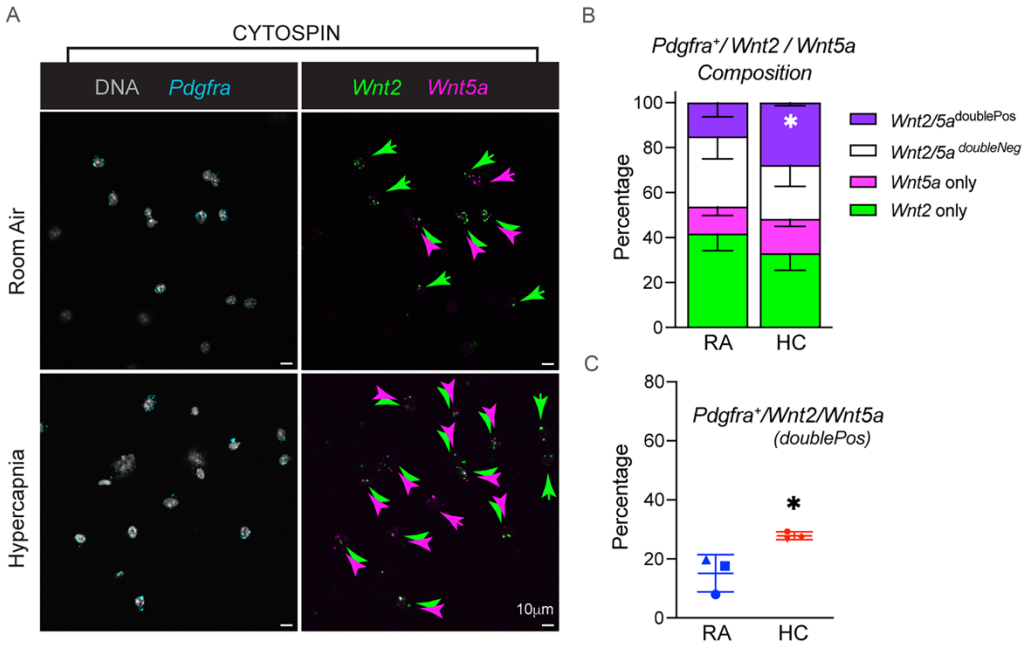

Figure 8. PDGFRα^{+} flow-sorted fibroblasts show non-uniform expression of *Wnt2* and *Wnt5a*. (A) Confocal images of PDGFRα flow-sorted fibroblasts isolated from Room Air (RA) and hypercapnia (HC) exposed mice for 10 days were subjected to cytospin/RNA-FISH analysis with probes for *Pdgfra* (cyan), *Wnt2* (green) and *Wnt5a* (magenta). Nuclei in gray. RNA-FISH signal intensity converted to object spots to measure co-occurrence of *Wnt2, Wnt5a* or both signals within the *Pdgfra* signal region. Colored arrows denote single Wnt and double-Wnt-positive cells. Scale bars:10 μm. (**B and C**) Graphical representation of the percentage of *Wnt2* or *Wnt5a* single positive versus double-positive *Pdgfra*$^{+}$ cells. n=3 (each point consists of three mice), 3 fields of view/mouse with more than 400 measurements per condition. ***P*<0.01.

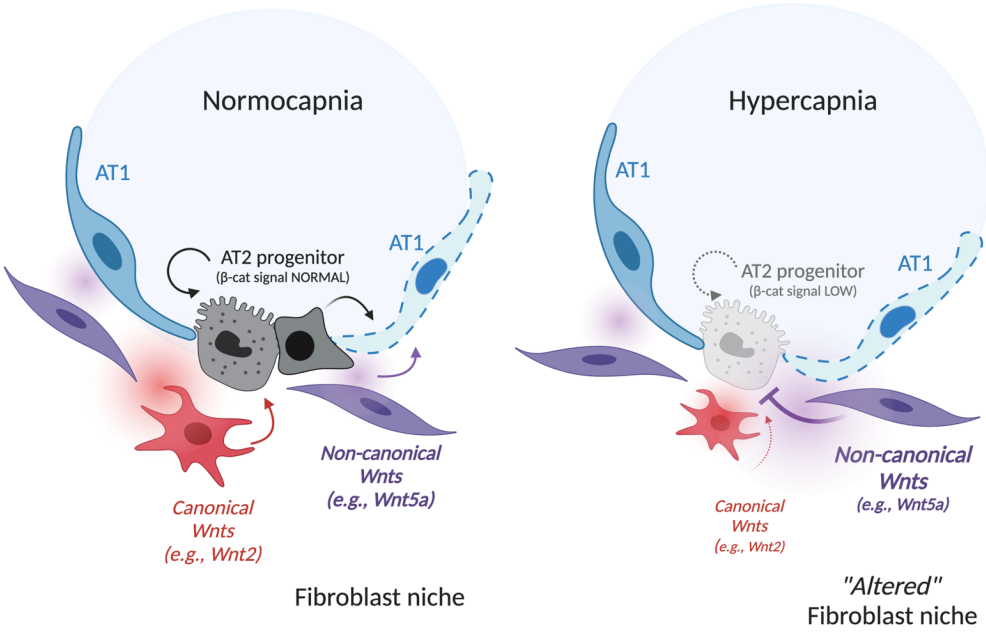

Figure 9. Model for hypercapnia-mediated inhibition of βcat signaling in AT2 cells via skewing of fibroblast-derived Wnts. Left) Normocapnia: AT2 progenitors are spatially proximal to *Pdgfra/Wnt2*-expressing fibroblasts (red/red gradient) that maintain βcat signaling and AT2 self-renewal to replace damaged AT1 cells. *Pdgfra/Wnt5a*-expressing fibroblasts (purple/purple gradient) are spatially further from the AT2 cell, perhaps to ensure separation of competing βcat-activating (WNT2) from βcat-inhibiting (WNT5A) signals. **Right**). Hypercapnia leads to reduced βcat signaling in AT2 cells, impairing cell renewal and differentiation by skewing Wnt expression in PDGFRα-stromal cells towards a non-canonical variety, with *Wnt5a* significantly elevated. Narrowness of the AT2 progenitor niche raises possibility that elevated WNT5A release (purple gradient) in close spatial vicinity to the WNT2 signal (red gradient) antagonizes βcat signaling in AT2 cells, which inhibits proliferative capacity.